JACS
JOURNAL OF THE AMERICAN CHEMICAL SOCIETY
Article
pubs.acs.org/JACS

Low-Potential Sodium Insertion in a NASICON-Type Structure through the Ti(III)/Ti(II) Redox Couple

P. Senguttuvan,[†,‡] G. Rousse,[§] M. E. Arroyo y de Dompablo,[∥] Hervé Vezin,[⊥] J.-M. Tarascon,[‡] and M. R. Palacín*[,†]

[†]Institut de Ciència de Materials de Barcelona (ICMAB-CSIC), ALISTORE ERI European Research Institute, Campus de la Universitat Autònoma de Barcelona (UAB), E-08193 Bellaterra, Catalonia, Spain

[‡]Laboratoire de Réactivité et Chimie des Solides, Université de Picardie Jules Verne (UPJV), CNRS UMR-6007, ALISTORE ERI European Research Institute, 33 rue Saint Leu, 80039 Amiens, France

[§]Institut de Minéralogie et de Physique des Milieux Condensés (IMPMC), UMR 7590 CNRS, Université Pierre et Marie Curie UPMC Univ Paris 06, Case courrier 115, 4 Place Jussieu, 75252 Paris Cedex 05, France

[∥]Departamento de Química Inorgánica, Universidad Complutense de Madrid, 28040 Madrid, Spain

[⊥]Université Lille Nord de France, CNRS, UMR 8516-LASIR, Univ Lille 1, F-59655 Villeneuve d'Ascq, France

Supporting Information

ABSTRACT: We report the direct synthesis of powder $Na_3Ti_2(PO_4)_3$ together with its low-potential electrochemical performance and crystal structure elucidation for the reduced and oxidized phases. First-principles calculations at the density functional theory level have been performed to gain further insight into the electrochemistry of Ti(IV)/Ti(III) and Ti(III)/Ti(II) redox couples in these sodium superionic conductor (NASICON) compounds. Finally, we have validated the concept of full-titanium-based sodium ion cells through the assembly of symmetric cells involving $Na_3Ti_2(PO_4)_3$ as both positive and negative electrode materials operating at an average potential of 1.7 V.

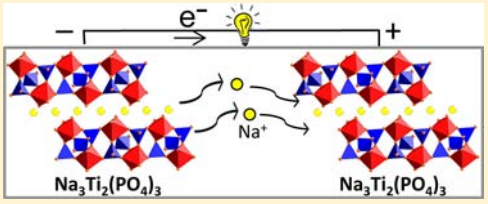

INTRODUCTION

The mature lithium ion battery technology has been key in the development of portable electronics in the past and is currently starting to enter the electric vehicle propulsion field. With the aim of achieving similar progress in other domains of application, researchers are now exploring alternative electrochemical energy storage technologies such as the analogous sodium ion technology. The idea was developed in the early days of intercalation studies[1,2] but mainly abandoned at the point when attractive performance was achieved[3] due to the much higher intrinsic energy density for lithium-based systems. Still, the concept survived[4] and is currently again capturing the attention of the scientific community as a sustainable lower cost alternative to the lithium ion technology, especially with prospects in stationary applications for which cost rather than energy density is the top priority.[5−11]

While a variety of phases that can potentially be used as positive electrodes in sodium ion batteries have been reported, the choice on the negative side is much more restricted. While Na-alloying anodes begin to emerge, hard carbon[12,13] is currently the most commonly used one and has allowed the proof of concept for the Na ion technology. Even though enhanced performance has recently been reported,[14] its potential versus composition profile exhibits a plateau very close to 0 V, which may raise safety concerns at high rates due to risk of sodium plating. Besides, an inherent issue to carbon is its low density (~1.70 g/cm^3), which results in low volumetric specific capacity. When it comes to transition-metal oxides as an alternative, the choice is rather limited owing to the competition of insertion vs conversion[15] reactions, the former only being favored for early 3d metal oxides. We recently identified $Na_2Ti_3O_7$ as an effective low-potential insertion sodium compound owing to its ability to reversibly uptake two Na ions per formula unit (200 mAh/g) at a surprisingly low average potential of 0.3 V through a two-phase redox mechanism involving the Ti(IV)/Ti(III) couple.[16] Such low-potential operation for a somewhat dense material (3.4 g/cm^3) being beneficial in terms of energy density, the quest for other materials exhibiting this feature is challenging. The low Ti(IV)/Ti(III) potential within $Na_2Ti_3O_7$ is rooted in the structural rearrangement involved in the redox mechanism,[17] which may also contribute to the important capacity fading observed upon cycling. Alternatively, targeting phases involving the Ti(III)/Ti(II) redox couple within a stable crystal framework seems a priori an interesting strategy to keep lower potential operation while preventing capacity fading upon cycling. Such low oxidation states have been reported for titanium,[18] and lithium insertion concomitant to Ti(III) reduction to Ti(II) has been reported in $LiTiS_2$.[19]

Among structural frameworks suitable to stabilize the Ti(III)/Ti(II) couple through sodium intercalation at low

Received: November 9, 2012
Published: February 19, 2013

   dx.doi.org/10.1021/ja311044t | J. Am. Chem. Soc. 2013, 135, 3897−3903

potential, the sodium superionic conductor (NASICON) structure appears as the first choice. It consists of 3D strongly bonded "lantern" structural units consisting of three XO_4 tetrahedra connected to two MO_6 octahedra, with alkaline ions sitting in the large interstitial positions. The large possible composition spectrum involving different elements within the M and X positions was used by J. B. Goodenough and co-workers[20,21] to exemplify how the M redox transition-metal potentials can be tuned through the control of the ionocovalency of M−O bonds by the strength of the inductive effect from XO_4 tetrahedra, which is in turn determined by the electronegativity of X. $Na_3Ti_2(PO_4)_3$ has been known for more than 30 years, its preparation, crystal chemistry, magnetic properties, and electrochemistry having been reported by Delmas and co-workers.[22−26] However, no attempt has been reported to reduce this or any other related phase to Ti(II). The reported Ti(IV)/Ti(III) couple at a potential of 2.1 V vs Na^+/Na^0 and the ca. 1.8 V voltage differences observed between V(IV)/V(III) and V(III)/V(II) redox couples within $Na_3V_2(PO_4)_3$[27,28] allow us to believe in the feasibility of reaching the Ti(III)/Ti(II) couple.

Besides targeting low-voltage intercalation, a major advantage of titanium-based compounds when compared to their vanadium analogues is their lower cost and the fact that they are environmentally benign.

EXPERIMENTAL SECTION

$Na_3Ti_2(PO_4)_3$ was prepared from a 1 g stoichiometric mixture of NaH_2PO_4 (Sigma-Aldrich, 99%) and TiO_2 (Sigma-Aldrich, 99.9%) in a 3:1 molar ratio which was ball milled with a high-energy SPEX 800 miller for 30 min. The reactant mixture was treated at 350 °C for 3 h in air to eliminate water and further heated at 650 °C in an Ar/H_2 mixture with 10% H_2 (v/v) for 48 h with an intermittent regrinding. Since the compound is moisture sensitive, all manipulations were performed in an Ar-filled glovebox.

Powder X-ray diffraction (XRD) patterns were obtained with a Bruker D8 diffractometer, equipped with a Cu Kα radiation source (λ_1 = 1.54056 Å, λ_2 = 1.54439 Å) and a Lynxeye detector. A homemade Swagelok-type cell using a Be window[29] was used as the sample holder for data acquisition to avoid exposure to air. Additional high-resolution synchrotron powder diffraction patterns were collected on some samples sealed under Ar in glass capillaries with a 0.5 mm diameter at the 11-BM beamline (λ = 0.41329 Å) at the Advanced Photon Source (Argonne National Laboratory, mail-in program). Rietveld[30] refinements were done using the FullProf program.[31]

Energy-dispersive spectrometry (EDS) analysis was carried out on an FEI Quanta 200F SEM microscope.

Electrochemical tests were performed in either two- or three-electrode Swagelok cells. Half-cells were assembled using a sodium metal cube slice (Aldrich, 99.95%) as the counter electrode. Symmetric full cells were also assembled with an electrode mass balance of 0.5 between the positive and the negative sides. Two sheets of Whatman GF/D borosilicate glass fiber were used as the separator, soaked with 1 M $NaClO_4$ in propylene carbonate (PC) electrolyte. The cells were tested using a MacPile potentiostat (Bio-Logic, France). The working electrode consisted of ca. 5−6 mg of a powder mixture of the active material with 30% carbon black (Super P, Timcal, Switzerland). The performance was evaluated through galvanostatic cycling with potential limitation (GCPL) experiments at C/25. Chemical oxidation of 500 mg of $Na_3Ti_2(PO_4)_3$ for comparative purposes has been carried out in acetonitrile using NO_2BF_4 as the oxidizing agent (50% molar excess with respect to $Na_3Ti_2(PO_4)_3$). The suspension was stirred for 3 days at room temperature inside an argon-filled drybox, and the resulting powder was recovered by centrifugation and washed twice with acetone.

X-band electron paramagnetic resonance (EPR) experiments were carried out at 4.2 K using a Brüker ELEXSYS II E580. The modulation amplitude and microwave power were set respectively to 5 G and 1 mW. The pristine and electrochemically reduced samples were sealed inside a quartz tube under 10^{-5} bar for EPR measurement. The quantification of paramagnetic species was done with the double-integration spectrum procedure, corrected and normalized to the weight of each compound.

The total energies of $Na_3Ti_2(PO_4)_3$, $NaTi_2(PO_4)_3$, and $Na_4Ti_2(PO_4)_3$ have been calculated using the ab initio total-energy and molecular dynamics program VASP (Vienna ab initio simulation program) developed at the Universität Wien.[32,33] Total energy calculations based on the density functional theory (DFT) were performed within the general gradient approximation (GGA), with the exchange and correlation functional form developed by Perdew, Burke, and Ernzerhof (PBE).[34] The interaction of core electrons with the nuclei is described by the projector augmented wave (PAW) method.[35] The total energy of pristine, oxidized, and reduced phases was also computed within the GGA+U method with an effective U value of 4 eV for Ti ions. The energy cutoff for the plane wave basis set was kept fixed at a constant value of 600 eV throughout the calculations. The integration in the Brillouin zone is done on a set of k points (2 × 2 × 1) determined by the Monkhorst−Pack scheme. A convergence of the total energy close to 10 meV per formula unit is achieved with such parameters. The initial cell parameters and atomic positions of $Na_3Ti_2(PO_4)_3$ were taken from the work by Kabbour et al.,[36] with the unit cell containing six formula units ($Na_{18}Ti_{12}(PO_4)_{18}$). Crystallographic details for the oxidized $NaTi_2(PO_4)_3$ and reduced $Na_4Ti_2(PO_4)_3$ phases have been extracted from the present experimental work. Spin-polarized calculations were performed.

RESULTS AND DISCUSSION

The structure of $Na_3Ti_2(PO_4)_3$ was examined through Rietveld refinement of its synchrotron X-ray powder diffraction pattern. The crystal structure of $Na_3Ti_2(PO_4)_3$ has recently been revisited,[36] and the results of single-crystal X-ray diffraction allowed a 30 year old controversy about the position of the sodium atoms in the NASICON framework to be ended. The structure was originally reported[21] as rhombohedral, with space group $R\bar{3}c$, assuming that sodium ions are distributed among two crystallographic sites (see the inset in Figure 1): M(1) between two TiO_6 octahedra along the c-axis, fully occupied, and M(2) with 8-fold coordination with an occupation factor of 2/3. M(1) corresponds to the 6b (0,0,0) Wyckoff position, and M(2) corresponds to the 18e Wyckoff position (x,0,1/4) of $R\bar{3}c$. Kabbour's single-crystal study indicates that the real symmetry of the unit cell is triclinic, with an ordering of Na ions and vacancies within the M(2) site.

We have done the structural refinement of the as-prepared $Na_3Ti_2(PO_4)_3$ phase using synchrotron XRD data using the two models mentioned above: Our results using the two structural models (see Figure 1) clearly confirm that the $R\bar{3}c$ space group assignment is wrong. Indeed, the (003) reflection at 3.28° is clearly visible, as pointed out by Aatiq for the lithium analogue.[37] On the contrary, there is good agreement between the observed and calculated patternd for the model with triclinic symmetry, even without refining any of the atomic positions, and hence, the validity of the structure published from single-crystal diffraction[36] is fully confirmed through powder diffraction. Moreover, a splitting of the peaks as a consequence of the triclinic symmetry can be clearly seen for synchrotron diffraction data, which was not detected through laboratory X-ray diffraction due to a less accurate instrumental resolution. The lattice parameters of $Na_3Ti_2(PO_4)_3$ in the triclinic structure are reported in Table 1.

Figure 2a shows the potential versus composition profile for $Na_3Ti_2(PO_4)_3$ cycled against sodium metal in galvanostatic

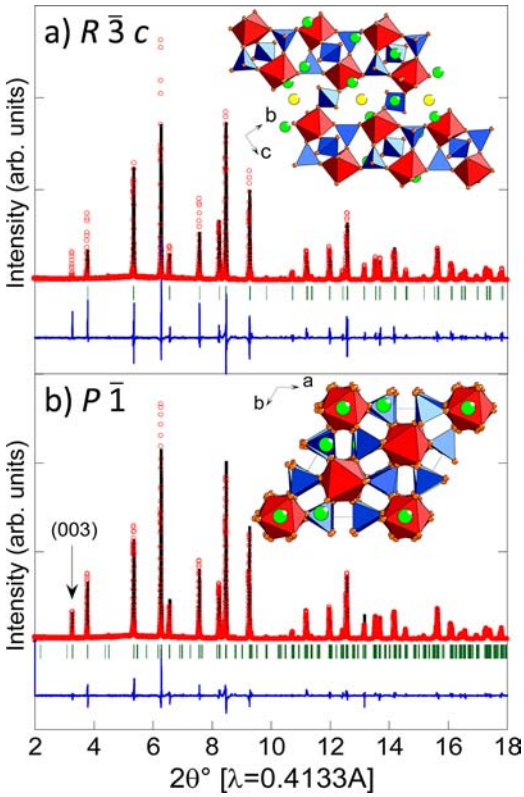

Figure 1. Rietveld refinements of the 11-BM synchrotron X-ray diffraction pattern of as-made $Na_3Ti_2(PO_4)_3$ (λ = 0.4133 Å): (a) with the average $R\bar{3}c$ structure, (b) using the triclinic structural model of Kabbour et al.[36] Red circles and black and blue lines represent the observed, calculated, and difference patterns, respectively. The green tick marks correspond to the Bragg reflections. The structure is displayed as an inset (top, perpendicular to the *a* axis; bottom, perpendicular to the *c* axis of the unit cell). TiO_6 octahedra are red, PO_4 tetrahedra are blue, and sodium ions are distributed among two sites: M(1), fully occupied (yellow balls), and M(2), which is occupied 2/3 by sodium ions and 1/3 by vacancies (green balls) which are ordered in the triclinic cell.

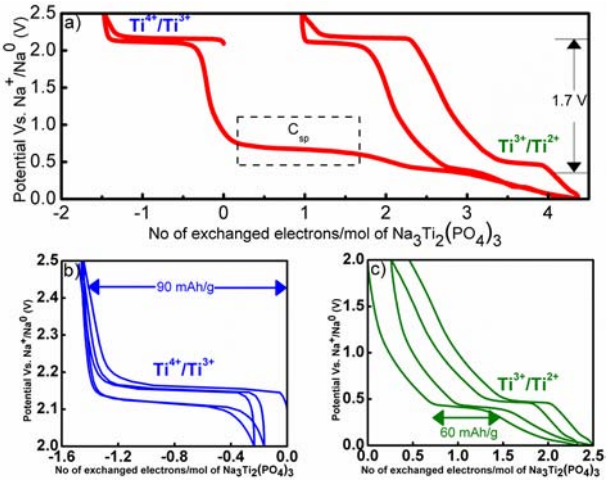

Figure 2. Galvanostatic cycling of $Na_3Ti_2(PO_4)_3$ vs Na between 2.5 and 0 V for the first charge/discharge and subsequent charge/discharge (a). Then two cells were assembled and cycled around the 2.1 and 0.4 V plateaus as shown in (b) and (c), respectively. Note that we reported on the abscissa the number of exchanged electrons per $Na_3Ti_2(PO_4)_3$ and not the number of sodiums in $Na_{3\pm x}Ti_2(PO_4)_3$ as usual because of the irreversible contribution of carbon at 0.7 V and of electrolyte at low potential, which adds extra capacity so that all the exchanged electrons are not used for sodium insertion into the $Na_3Ti_2(PO_4)_3$ framework . For more information see the text.

mode at a C/25 rate between 2.5 and 0 V. Upon oxidation, a plateau at ca. 2.1 V vs Na^+/Na^0 is observed, corresponding to the oxidation of ca. 75% of Ti(IIII) to Ti(IV), which appears to be reversible upon subsequent reduction. When further reduction to lower potentials is attempted, two additional plateaus are observed located respectively at 0.8 and 0.4 V, most likely corresponding to the irreversible reaction of sodium with carbon black[16] and the reduction of Ti(III) to Ti(II), respectively. In agreement with this, only the 2.1 and 0.4 V plateaus are observed upon further oxidation and subsequent cycles. The tentative adscription of the processes taking place at 2.1 and 0.4 V to the Ti(IV)/Ti(III) and Ti(III)/Ti(II) redox

Table 1. Structural Parameters Deduced from Rietveld Refinements for Pristine $Na_3Ti_2(PO_4)_3$, $NaTi_2(PO_4)_3$ Prepared through Chemical Oxidation of $Na_3Ti_2(PO_4)_3$ (11-BM Synchrotron XRD Data), and $Na_4Ti_2(PO_4)_3$ Prepared through Electrochemical Reduction of $Na_3Ti_2(PO_4)_3$ (Laboratory XRD Data)[a]

	pristine $Na_3Ti_2(PO_4)_3$	chem oxidized $NaTi_2(PO_4)_3$	electrochem reduced $Na_4Ti_2(PO_4)_3$
space group	$P\bar{1}$	$R\bar{3}c$	$R\bar{3}c$
a (Å)	8.8647(1) (8.942; 9.011)	8.4892(1) (8.614; 8.642)	9.0570(5) (9.138; 9.226)
b (Å)	8.8662(1) (8.949; 9.025)		
c (Å)	21.6274(1) (21.653; 21.702)	21.7856(1) (21.905; 22.054)	21.382(1) (21.246; 21.424)
angles (deg)	α = 89.877(1) (90.10; 90.14)		
	β = 90.151(1) (90.00; 90.00)		
	γ = 120.117(1) (119.98; 119.95)		
volume (Å^3)	1470.35(2) (1500.92; 1529.53)	1359.666(5) (1407.80; 1426.51)	1518.990(8) (1536.43; 1577.99)
M(1) 6*b* Wyckoff site occ factor	τ = 1	τ = 1	τ = 1
M(2) 18*e* Wyckoff site occ factor	τ = 2/3 ordering of Na/vacancies	τ = 0	τ = 1
Ti−O av distance (Å)	2.029(3) (2.058; 2.088)	1.931(1) (1.9570; 1.976)	2.123(6) (2.1121; 2.1536)
BVS on Ti atoms	+3.08(1)	+3.69(4)	+2.54(4)
reliability factors	R_{Bragg} = 6.23%, χ^2 = 3.53	R_{Bragg} = 4.57%, χ^2 = 2.73	R_{Bragg} = 2.47%, χ^2 = 3.91

[a]Occupation factors for both M(1) and M(2) sites are available for sodium ions. Ti−O average distances and bond valence sum (BVS) on titanium atoms deduced from the refinement are also given. For pristine $Na_3Ti_2(PO_4)_3$, this value is the mean over the six values obtained on the six independent positions for Ti in the $P\bar{1}$ structure. Calculated lattice parameters and distances within the DFT are given in parentheses (GGA; GGA +*U*).

dx.doi.org/10.1021/ja311044t | J. Am. Chem. Soc. 2013, 135, 3897−3903

couples, with a 1.7 V difference between them, is in agreement with the 1.8 V difference observed for the vanadium counterpart system having a NASICON framework.[27,28] The first plateau (Figure 2b) shows a reversible and sustained capacity of 1.5 sodium ions per formula unit. This value increases to 1.8 by diminishing the cycling rate to C/50. Such values are in agreement with previous observations for the NASICON $Li_3Ti_2(PO4)_3$ phase, also exhibiting a capacity of 1.7 mol of lithium atoms per formula unit at a C/40 rate.[37] The low-voltage plateau (Figure 2c) exhibits a capacity close to 1 mol of sodium ions per formula unit but is much less well-defined owing on the upper side to some reactivity with sp carbon and on the lower side to pronounced electrolyte decomposition as indicated by the continuous voltage decay down to 0 V. Such electrolyte decomposition is most likely responsible for the limited capacity retention of the cells when cycled between 0 and 2 V vs Na^+/Na^0. For reasons not yet fully understood, low-potential intercalation oxides, $Na_2Ti_3O_7$ and also $Na_3Ti_2(PO_4)_3$, show poor capacity retention when cycled vs Na at lower C-rate, i.e., C/25 (Supporting Information, Figure S1) despite the fact that the volume change associated with this plateau is less than 4% for the NASICON phase. This is in contrast with excellent capacity retention displayed by hard C/Na cells. Such a comparison suggests an enhanced catalytic activity of these Ti-based phases toward electrolyte decomposition which must be explored further. To test this hypothesis, we have increased the cutoff voltage and C-rate to 0.3 V and C/10, respectively, and found better capacity retention.

To further understand the structural evolution of $Na_3Ti_2(PO_4)_3$ upon sodium deinsertion and reinsertion, the electrochemical reaction was followed through in situ X-ray diffraction. Figure 3b exhibits XRD patterns taken upon

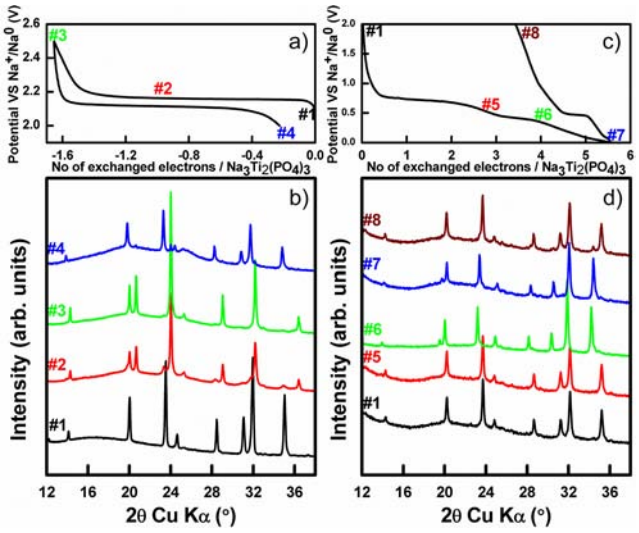

Figure 3. XRD diffraction patterns (Cu Kα) recorded in situ at different stages of the galvanostatic cycling of $Na_3Ti_2(PO_4)_3$ upon oxidation (a,b) and reduction (c,d).

oxidation (at points labeled 1−4 in Figure 3a). Upon sodium removal a new set of peaks appear at 2θ = 20.7°, 24.1°, 29.3°, and 32.3° which grow in intensity (Figure 3b, pattern 2) at the expense of the pristine one. The pattern becomes single phase when 1.7 sodium ions are removed from the structure (Figure 3b, pattern 3). Starting from the average structure described in $R\bar{3}c$, we refined the pattern corresponding to the fully oxidized phase (Figure 3b, pattern 3) with three models (see the Supporting Information, Figure S2): sodium ions extracted only from the M(1) site, only from the M(2) site, or statistically from both sites. These three models lead to patterns that differ in the relative peak intensities. We found that removing Na from the M(2) site only gives the best agreement with the observed pattern.

To further confirm this model, synchrotron X-ray diffraction was carried out on the chemically oxidized $Na_xTi_2(PO_4)_3$. The x value was determined by EDS measurement to be close to 1 (e.g., $Na_1Ti_2(PO_4)_3$). Its pattern exhibits very narrow peaks which can be indexed with a rhombohedral cell ($R\bar{3}c$ space group). We refined the occupation factors of the M(1) and M(2) sites sequentially and found that sodium ions in $NaTi_2(PO_4)_3$ are solely on the M(1) site and the M(2) site is empty, which is in agreement with the composition of the fully oxidized phase being $NaTi_2(PO_4)_3$. The obtained structure is therefore similar to the structure proposed by Delmas et al.[25] with no sign of triclinic distortion as in $Na_3Ti_2(PO_4)_3$. This comes as no surprise since the triclinic cell of $Na_3Ti_2(PO_4)_3$ arises from sodium/vacancies ordering, and removing Na from the M(2) site destroys this ordering. The corresponding Rietveld refinement is shown in the Supporting Information, Figure S3, and the structural parameters are given Table 1.

The XRD pattern of the electrochemically oxidized sample can also be fitted with this structural model, as can be seen from Figure 4a. As the beryllium window makes the pattern free of

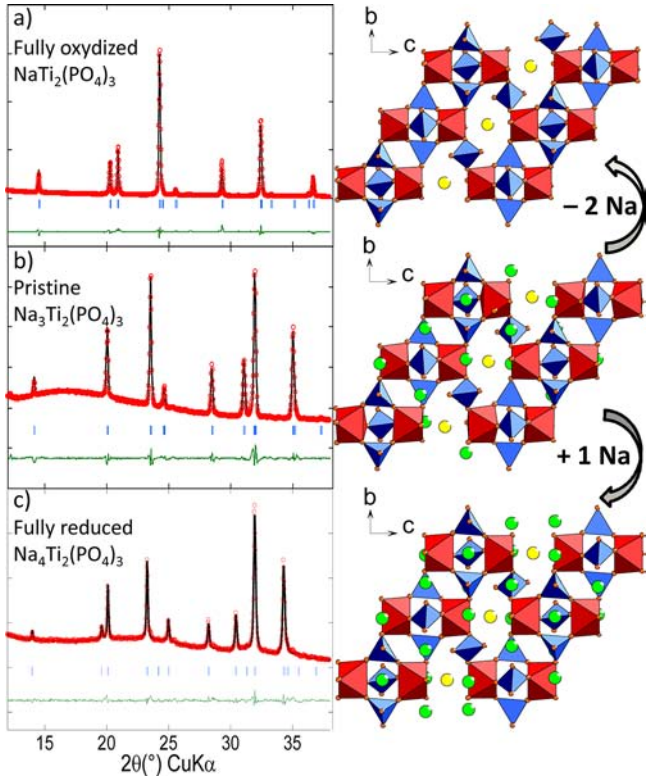

Figure 4. Rietveld refinement of (a) electrochemically oxidized $NaTi_2(PO_4)_3$, (b) pristine $Na_3Ti_2(PO_4)_3$, and (c) electrochemically reduced $Na_4Ti_2(PO_4)_3$. Red circles and black and blue lines represent the observed, calculated, and difference patterns, respectively (λ_{Cu}). The green tick marks correspond to the Bragg reflections. The corresponding structures are displayed in the right panel.

dx.doi.org/10.1021/ja311044t | J. Am. Chem. Soc. 2013, 135, 3897−3903

Table 2. Structural Parameters and Bond Valence Sum (BVS) for Electrochemically Reduced $Na_4Ti_2(PO_4)_3$ Obtained from Rietveld Refinement of the in Situ XRD Data (Laboratory XRD Data)[a]

atom	Wyckoff site	occ factor	x	y	z	BVS
Na1	6*b* M(1)	1	0	0	0	1.12(2)
Na2	18*e* M(2)	1	0.645(1)	0	1/4	0.84(2)
Ti	12*c*	1	0	0	0.147(1)	2.54(4)
P	18*e*	1	0.297(1)	0	1/4	4.88(11)
O1	36*f*	1	0.186(1)	−0.026(2)	0.189(1)	1.75(4)
O2	36*f*	1	0.331(2)	0.854(1)	0.247(1)	2.14(8)

[a]Space group $R\bar{3}c$, lattice parameters a = 9.0570(5) Å and c = 21.382(1) Å.

any valuable information after $2\theta = 40°$ (λ_{Cu} = 1.5418 Å), the scale factor was first refined together with the peak profile and lattice parameters. Second, the atomic positions were refined, making sure that they do not give unrealistic values. In particular, we paid special attention to the bond valence sum (BVS) analysis deduced from the Rietveld refinement employing the formula $V_i = \sum_j s_{ij} = \sum_j \exp((d_0 - d_{ij})/0.37)$ using the d_0 parameter taken from ref 38. The BVS obtained for the titanium atom is displayed in Table 1, and the value obtained is in full agreement with titanium being oxidized to +4 as compared to that in the pristine $Na_3Ti_2(PO_4)_3$, for which the BVS is also indicated in Table 1. Figure 4b presents the refinement of data corresponding to pristine $Na_3Ti_2(PO_4)_3$ taken in the same conditions (behind a beryllium window) with the average $R\bar{3}c$ model. Upon sodium extraction, the c lattice parameter increases as a result of the stronger electrostatic repulsion between adjacent Ti(IV) ions which are not screened by Na ions, in agreement with previous reports.[25] We should note that such a Na removal also corresponds to a 7.5% volume change, which is along the line of what can be tolerated for application.

XRD patterns from samples at different stages of oxidation depicted in Figure 3b can be successfully fitted considering a mixture of both end phases. An example of refinement is shown (see the Supporting Information, Figure S4) for a pattern recorded in the middle of the 2.1 V plateau (Figure 3b, pattern 2) which can be fitted with 40 wt % pristine $Na_3Ti_2(PO_4)_3$ and 60 wt % $NaTi_2(PO_4)_3$. These results are consistent with the redox process being two-phase as deduced from the sharp peak in the derivative dx/dV curve (Supporting Information, Figure S1).

Let us turn now to the insertion of sodium into pristine $Na_3Ti_2(PO_4)_3$ upon reduction. From the potential vs composition curve (Figure 2c, from second cyle) ca. 1 mol of sodium ions per formula unit can be inserted into $Na_3Ti_2(PO_4)_3$, which leads to the formation of $Na_4Ti_2(PO_4)_3$. Figure 3d shows the XRD patterns collected at different stages of cycling (indicated by numbers in Figure 3c) between 2.0 and 0.0 V. No significant difference can be found between pattern number 5 and that of the pristine phase (number 1), which again proves that the first redox feature corresponds to sodium ions reacting solely with carbon. Further reduction resulted in the growth of a new phase with the major peaks located at 2θ = 20.1°, 23.3°, 28.1°, 30.4°, 39.9°, and 34.3° which becomes single phase after the uptake of 1 mol of sodium ions per formula unit, leading to a composition close to $Na_4Ti_2(PO_4)_3$. Pushing the reduction down to 0 V results in a continuous voltage decay due to electrolyte decomposition, in agreement with the XRD pattern of the $Na_4Ti_2(PO_4)$ phase not changing at all in this region. NASICON phases with the composition $Na_4M_2(PO_4)_3$ were previously reported for M = V[27] and M = Fe,[39] but never reported to our knowledge for M = Ti. Due to the larger size of sodium ions, they cannot enter the M(3) sites (available for lithium ions), which are located on the side of the M(2) sites.[37] Therefore, the only possibilities for inserting additional sodium ions are the vacancies on the M(2) site and the 6*a* Wyckoff site. However, the latter would induce very small Na−Ti distances (about 2.3 Å), and hence, this hypothesis is very unlikely.

Fully reduced $Na_3Ti_2(PO_4)_3$ recovered from the electrochemical cell was sealed inside a capillary under argon, but the sample was very reactive and reoxidized very quickly, so all attempts to measure the synchrotron X-ray diffraction pattern of pure $Na_4Ti_2(PO_4)_3$ failed. We thus decided to test structural models directly using in situ laboratory XRD patterns refining only lattice parameters. The best agreement with the experimental pattern was found when the M(2) site is fully filled with sodium ions, in agreement with the formula $Na_4Ti_2(PO_4)_3$ with mixed valence Ti(II)/Ti(III) (Figure 4c). Refined lattice parameters of this inserted phase are reported in Table 1, and the atomic positions are reported in Table 2.

The BVS obtained from the refinement indicates that Ti is at an oxidation state of roughly +2.5, as expected. The evolution of the lattice parameters upon sodium insertion from $NaTi_2(PO_4)_3$ to $Na_4Ti_2(PO_4)_3$ follows a behavior similar to that pointed out and explained by Hatert[39] and Masquelier[40] for the iron analogue: c decreases due to the reduction of electrostatic repulsion, the M(2) site is fully occupied, and a increases as a result of the reduction of Ti to the (II) oxidation state.

Low-temperature EPR experiments were performed to probe the existence of Ti(II) in the reduced electrode battery material. As Ti(III) is a d_1 paramagnetic ion, it has a g factor value below that of a free electron which is g = 2.0023. For quantification of the Ti(III) amount in the reduced phase, we use pristine $Na_3Ti_2(PO_4)_3$ as a reference.

The results displayed in Figure 5 show that the pristine spectrum exhibits a broad signal of 500 G centered at g = 1.84 with a weak anisotropy. This signal is typical of Ti(III) species. For the fully reduced sample we can also see signals with a line width of 200 G centered at g = 1.94. According to the double-integration procedure, the amount of the Ti(III) in the reduced sample was estimated as nearly 50% of the pristine sample, in agreement with 50% of Ti(III) being converted to Ti(II) (EPR silent) upon reduction.

Once the sodium insertion process into $Na_3Ti_2(PO_4)_3$ was understood, it was then tempting to try to build a symmetric cell having identical electrodes to start with as has been done in the past[41] with $LiMn_2O_4$,[42] $LiVPO_4F$,[43] or $Na_3V_2(PO_4)_3$,[38] which also possess two plateaus separated by 1, 2.4, and 1.8 V, respectively. To optimize the performance of such a cell, a three-electrode Swagelok configuration[44] was used to monitor

dx.doi.org/10.1021/ja311044t | J. Am. Chem. Soc. 2013, 135, 3897−3903

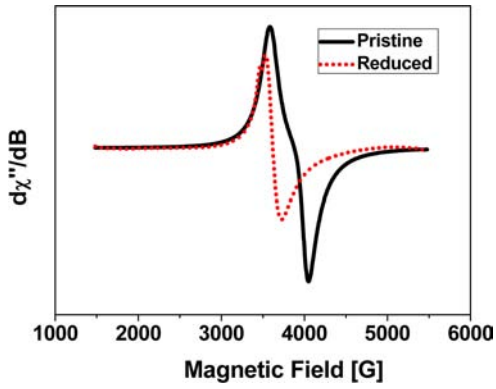

Figure 5. EPR spectra of $Na_3Ti_2(PO_4)_3$ pristine and after electrochemical reduction to $Na_4Ti_2(PO_4)_3$.

of the potential of each electrode ss Na^+/Na^0 as well as the output cell voltage.

$Na_3Ti_2(PO_4)_3$ therefore presents an added difficulty due to (i) the moisture sensitivity of the as-made material and (ii) the large amount of irreversible capacity due to carbon when the compound is cycled over the low-voltage plateau, which renders cell balancing complicated. To alleviate this issue, we first made a NASICON/Na cell that we cycled between 2 and 0 V, stopped during the second charge cycle at 0.5 V, and opened within the drybox to recover the cathode film. This film was then used as the negative electrode in a sodium ion cell using pristine $Na_3Ti_2(PO_4)_3$ as the positive electrode. The voltage window of the symmetric cell was controlled by the positive electrode cutoff voltage as 2.6−1.9 V vs Na^+/Na^0, and the potential profile for such a sodium ion cell is shown in Figure 6. The cell exhibits an open circuit voltage of 1.5 V, consistent with the different potentials of the positive and negative electrodes. Although the capacity upon cycling is preserved for the positive electrode, we note small changes in the $V = f(x)$ curve of the symmetric cell, which could be due to the positive and negative electrode balance not being optimized and also the consumption of sodium ions to build the solid−electrolyte interphase layer upon cycling.

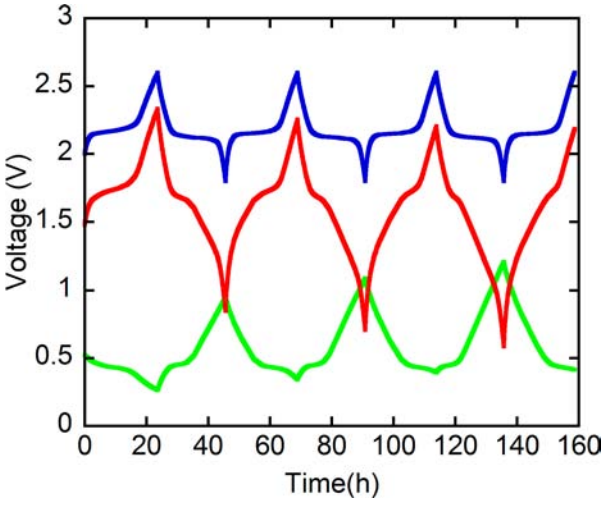

Figure 6. Potential profile as a function of time for symmetric $Na_3Ti_2(PO_4)_3$||$NaClO_4$ in PC||$Na_3Ti_2(PO_4)_3$ cells with a three-electrode configuration cycled at C/20 at room temperature. Mass loadings of the cathode and anode were 1.68 and 5.68 mg/cm^2, respectively. Blue and green voltage profiles represent the potentials of positive and negative electrodes vs Na^+/Na^0. The red voltage profile represents the voltage difference between positive and negative electrodes. For more information on cell assembly, refer to the text.

At this stage, moving back to fundamentals, a legitimate question deals with the potential value of the Ti(III)/Ti(II) redox couple in this structure. BVS calculations give some trends, but to gain a better insight into this issue, DFT calculations were undertaken.

The GGA to the DFT has been recently shown to efficiently reproduce the electrochemical behavior of titanium oxides as anodes for lithium batteries.[45,46] Interestingly, it has been predicted that Li intercalation into B-TiO_2 is thermodynamically possible up to a Li/Ti ratio of 1.25, at an open circuit voltage of about 0.5 V. This result makes plausible reduction of Ti(III) via Na intercalation in polyoxoanionic Ti-based compounds.

The calculated lattice parameters for $NaTi_2(PO_4)_3$, $Na_3Ti_2(PO_4)_3$, and $Na_4Ti_2(PO_4)_3$ are in good agreement with the experimental values (see Table 1), the error in volume calculations being around 4%. Experimental average Ti−O distances and their evolution upon Na content are also well reproduced with the DFT calculations. Na intercalation voltages have been calculated starting from the calculated total energies of the pristine, oxidized, and reduced forms following the methodology described by Ceder and coworkers.[47,48] The predicted potentials within the GGA are

$$NaTi_2(PO_4)_3 + 2Na \rightarrow Na_3Ti_2(PO_4)_3 \quad (1.19\,V) \qquad (1)$$

$$Na_3Ti_2(PO_4)_3 + Na \rightarrow Na_4Ti_2(PO_4)_3 \quad (0.36\,V) \qquad (2)$$

The calculated insertion voltage of reaction 1 is 0.9 V below the experimental value (2.1 V). This is not surprising; within the GGA-calculated voltages, deviation with respect to experimental values as large as 1.3 V has been reported for NASICON−$Li_3M_2(PO_4)_3$. The GGA+U method predicts a voltage of 2.12 V for reaction 1, which is in good agreement with experiments.

The calculated voltage for reaction 2 within the GGA is only 0.04 V below the experimental result. An analysis of the spin density around Ti ions reveals that in the reduced phase $Na_4Ti_2(PO_4)_3$ charge is delocalized between Ti cations, which have a formal oxidation state of $Ti^{2.5+}$. The reduction of Ti(III) is also predicted with the GGA+U method. The introduction of a Hubbard correction term (U_{eff} = 4 eV) in the calculation results in charge localization, so that the reduced phase can be formulated as $Na_4Ti^{3+}Ti^{2+}(PO_4)_3$. The calculated average voltage for reaction 2 is then 0.57 V, supporting that the experimentally observed electrochemical activity at 0.4 V is due to the reduction of Ti(III) to Ti(II). Interestingly, the experimental difference between Ti(IV)/Ti(III) and Ti(III)/Ti(II) redox couples of 1.7 V is better captured within the GGA +U (1.56 V) than within the GGA (0.86 V).

■ CONCLUSIONS

The feasibility of developing electrode materials for sodium ion batteries based on the Ti(III)/Ti(II) redox couple has been proved, and the structural changes associated with redox operation have been characterized through in situ and ex situ diffraction. Symmetric full-titanium-based sodium ion cells have been assembled which exhibit a moderate operation voltage. Overall, the results presented herein open new avenues in the quest for new negative electrode materials, for either sodium-

dx.doi.org/10.1021/ja311044t | J. Am. Chem. Soc. 2013, 135, 3897−3903

or lithium-based technologies targeting low oxidation states in transition-metal ions not prone to full reduction via conversion reactions.

■ ASSOCIATED CONTENT

Supporting Information

Derivative curves and plot of capacity upon cycling for symmetric cells together with simulated patterns for different M(2) occupations in the NASICON structure and additional Rietveld refinements. This material is available free of charge via the Internet at http://pubs.acs.org.

■ AUTHOR INFORMATION

Corresponding Author

rosa.palacin@icmab.es

Notes

The authors declare no competing financial interest.

■ ACKNOWLEDGMENTS

We acknowledge the Ministerio de Ciencia e Innovación (Spain) for Grant MAT2011-24757 and ALISTORE-ERI members for fruitful discussions. We also thank Lynn Ribaud for assistance in collecting data at the 11-BM line at Argonne National Laboratory. Use of the Advanced Photon Source at Argonne National Laboratory was supported by the U.S. Department of Energy, Office of Science, Office of Basic Energy Sciences, under Contract No. DE-AC02-06CH11357.

■ REFERENCES

(1) Whittingham, M. S. *Prog. Solid State Chem.* **1978**, *12*, 41.
(2) Abraham, K. M. *Solid State Ionics* **1982**, *7*, 199.
(3) Doeff, M. M.; Visco, S. J.; Ma, Y.; Peng, M.; De Jonghe, L. C. *Electrochim. Acta* **1995**, *40*, 2205.
(4) Barker, J.; Saidy, Y.; Swoyer, J. L. U.S. Patent 2002/0192553.
(5) Komaba, S.; Murata, W.; Ishikawa, T.; Yabuuchi, N.; Ozeki, T.; Nakayama, T.; Ogata, A.; Gotoh, K.; Fujiwara, A. *Adv. Funct. Mater.* **2011**, *21*, 3859.
(6) Ong, S. P.; Chevrier, V. L.; Hautier, G.; Jain, A.; Moore, C.; Kim, S.; Ma, X.; Ceder, G. *Energy Environ. Sci.* **2011**, *4*, 3680.
(7) Kim, D.; Kang, S. H.; Slater, M.; Rood, S.; Vaughey, J. T.; Karan, N.; Balasubramanian, M.; Johnson, C. S. *Adv. Energy Mater.* **2011**, *1*, 333.
(8) Palomares, V.; Serras, P.; Villaluenga, I.; Hueso, K. B.; Carretero-González, J.; Rojo, T. *Energy Environ. Sci.* **2012**, *5*, 5884.
(9) Slater, M.; Kim, D.; Lee, E.; Johnson, C. S. *Adv. Funct. Mater.* **2013**, *23*, 947.
(10) Kim, S. W.; Seo, D. H.; Ma, X.; Ceder, G.; Kang, K. *Adv. Energy Mater.* **2012**, *2*, 710.
(11) Ellis, B. L.; Nazar, L. F. *Curr. Opin. Solid State and Mater. Sci.* **2012**, *16*, 168.
(12) Stevens, D. A.; Dahn, J. R. *J. Electrochem. Soc.* **2000**, *147*, 4428.
(13) Stevens, D. A.; Dahn, J. R. *J. Electrochem. Soc.* **2001**, *148*, A803.
(14) Ponrouch, A.; Goni, A.; Palacin, M. R. *Electrochem. Commun.* **2013**, *27*, 85.
(15) Cabana, J.; Monconduit, L.; Larcher, D.; Palacin, M. R. *Adv. Mater.* **2010**, *12*, 315.
(16) Senguttuvan, P.; Rousse, G.; Seznec, V.; Tarascon, J. M.; Palacin, M. R. *Chem. Mater.* **2011**, *23*, 4109.
(17) Rousse, G.; Arroyo y de Dompablo, M. E.; Senguttuvan, P.; Tarascon, J. M.; Palacin, M. R. Manuscript in preparation.
(18) *Comprehensive Inorganic Chemistry*; Bailar, J. C., Emeleus, H. J., Nyholm, R., Trotman-Dickenson, A. F., Eds.; Pergamon Press: Oxford, U.K., 1973; Vol 3.
(19) Kim, Y.; Park, K. S.; Song, S. H.; Han, J. T.; Goodenough, J. B. *J. Electrochem. Soc.* **2009**, *156*, A703.
(20) Nanjundaswamy, K. S.; Padhi, A. K.; Goodenough, J. B.; Okada, S.; Ohtsuka, H.; Arai, H.; Yamaki, J. *Solid State Ionics* **1996**, *92*, 1.
(21) Padhi, A. K.; Nanjundaswamy, K. S.; Masquelier, C.; Goodenough, J. B. *J. Electrochem. Soc.* **1997**, *144*, 2581.
(22) Delmas, C.; Olazcuaga, R.; Cherkaoui, F.; Brochu, R.; Le Flem, G. *C. R. Acad. Sci.* **1978**, *287*, 169.
(23) Beltran-Porter, D.; Olazcuaga, R.; Delmas, C.; Cherkaoui, F.; Le Flem, G. *Rev. Chim. Miner.* **1980**, *17*, 458.
(24) Delmas, C.; Cherkaoui, F.; Nadiri, A.; Hagenmuller, P. *Mater. Res. Bull.* **1987**, *22*, 631.
(25) El Jazouli, A.; Nadiri, A.; Dance, J. M.; Delmas, C.; Le Flem, G. *J. Phys. Chem. Solids* **1988**, *49*, 779.
(26) Delmas, C.; Nadiri, A.; Soubeyroux, J. L. *Solid State Ionics* **1988**, *28−30*, 410.
(27) Plashnitsa, L. S.; Kobayashi, E.; Noguchi, Y.; Okada, S.; Yamaki, J. *J. Electrochem. Soc.* **2010**, *157*, A536.
(28) Jian, Z.; Zhao, L.; Pan, H.; Hu, Y. S.; Li, H.; Chen, S.; Chen, L. *Electrochem. Commun.* **2012**, *14*, 86.
(29) Morcrette, M.; Chabre, Y.; Vaughan, G.; Amatucci, G.; Leriche, J. B.; Patoux, S.; Masquelier, C.; Tarascon, J. M. *Electrochim. Acta* **2002**, *47*, 3137.
(30) Rietveld, H. M. *J. Appl. Crystallogr.* **1969**, *2*, 65.
(31) Rodriguez-Carvajal, J. *Physica B* **1993**, *192*, 55.
(32) Kresse, G.; Furthmuller, J. *Phys. Rev. B* **1996**, *54*, 169.
(33) Kresse, G.; Joubert, D. *Phys. Rev. B* **1999**, *59*, 1758.
(34) Perdew, J. P.; Burke, K.; Ernzerhof, M. *Phys. Rev. Lett.* **1996**, *77*, 3865.
(35) Bloch, P. E. *Phys. Rev. B* **1994**, *50*, 17953.
(36) Kabbour, H.; Coillot, D.; Colmont, M.; Masquelier, C.; Mentre, O. *J. Am. Chem. Soc.* **2010**, *133*, 11900.
(37) Aatiq, A.; Menetrier, M.; Croguennec, L.; Suard, E.; Delmas, C. *J. Mater. Chem.* **2002**, *12*, 2971.
(38) Brown, I. D.; Altermatt, D. *Acta Crystallogr., Sect. B: Struct. Commun.* **1985**, *41*, 244.
(39) Hatert, F. *Acta. Crystallogr., Sect. E: Struct. Rep. Online* **2009**, *65*, I30.
(40) Masquelier, C.; Wurm, C.; Rodríguez-Carvajal, J.; Gaubicher, J.; Nazar, L. *Chem. Mater.* **2000**, *12*, 525.
(41) Tarascon, J. M. *J. Electrochem. Soc.* **1985**, *132*, 2089.
(42) Li, W.; Dahn, J. R. *J. Electrochem. Soc.* **1995**, *142*, 1742.
(43) Plashnitsa, L. S.; Kobayashi, E.; Okada, S.; Yamaki, J. *Electrochim. Acta* **2011**, *56*, 1344.
(44) Guyomard, D.; Tarascon, J. M. *J. Eelectrochem. Soc.* **1992**, *139*, 937.
(45) Dalton, A. S.; Belak, A. A.; Van der Ven Chem, A. *Chem. Mater.* **2012**, *24*, 1568.
(46) Arrouvel, C.; Parker, S. C.; Islam, M. S. *Chem. Mater.* **2009**, *21*, 4778.
(47) Aydinol, M. K.; Kohan, A. F.; Ceder, G.; Cho, K.; Joannopoulos, J. *Phys. Rev. B* **1997**, *56*, 1354.
(48) Morgan, D.; Ceder, M.; Saidi, M. Y.; Barker, J.; Swoyer, J.; Huang, H.; Adamson, G. *Chem. Mater.* **2002**, *14*, 4684.